DEVELOPMENT OF A BIFURCATED JET FROM AN ELLIPTIC NOZZLE WITH ROUND CENTERBODY

David Munday[*] and Ephraim Gutmark[†],
University of Cincinnati

An elliptic nozzle with a conic centerbody has been found to generate a bifurcated jet. This behavior has been observed over a wide range of nozzle pressure ratios (NPRs) up to sonic and a heated condition as well as at room temperature. Particle Image Velocimitry (PIV) is used to track the development of the jet. Nozzle pressure ratios from 1.4 up to 1.89 and both hot (220F) and room temperature jets have been surveyed and the jet has been found to bifurcate under all surveyed conditions. Increasing Nozzle Pressure Ratio, or total temperature causes the bifurcated potential cores to be smaller and causes them to diverge from one another at a greater angle from the nozzle centerline. It is conjectured that this is purely a velocity effect. This effect is consistent but weak, however, and the dominant shapes of the velocity profiles change very little. In all cases the potential cores are extinct by $z = 1.9D_{eq}$ past the centerbody tip or $3.7D_{eq}$ past the nozzle exit plane. In all cases the potential cores become elongated, being longer in the major axis plane than in the minor axis plane.

Nomenclature

a	speed of sound
A	Exit area
D_{eq}	Equivalent diameter; $D_{eq} = 2\sqrt{A/\pi}$
h_1	Major axis exit height
h_2	Minor axis exit height
M	Mach number
NPR	Nozzle Pressure Ratio
T_0	Total Temperature
u_i	Ideal nozzle velocity (isentropic, quasi-1D)

[*] Graduate Student; member AIAA. *david.munday@uc.edu*
[†] Professor; Associate Fellow AIAA. *Ephraim.Gutmark@uc.edu*

Introduction

Jets are commonly used in applications where mixing and entrainment are desired. A detailed understanding of the development of jets is therefore desirable. Round jets have been well documented (Wygnanski & Fiedler 1969; Crow & Champagne 1971). Rectangular jets and elliptic jets (Krothapalli, Baganoff & Karamcheti 1981; Ho & Gutmark 1987) have been shown to greatly increase mixing. In some circumstances elliptic jets have been found to switch axes, enhancing mixing. Under other conditions elliptic jets have been found to bifurcate (Hussain & Husain 1989). The nozzle built for the present experiment was designed in anticipation of studying how the introduction of a centerbody influences axis switching. What we found instead is a bifurcation mechanism different from that observed by Hussain & Husain.

Hussain & Husain found that elliptic jets would switch axes at aspect ratios below four, and would bifurcate at aspect ratios above this value. Figure 1 from their paper shows the mechanism of axis switching and Figure 2 also from the same paper shows the mechanism for bifurcation. In both cases the mechanism is driven by vortex self induction, which varies with the radius of curvature of the vortex rings making up the high vorticity region in the shear layer.

Most of the published work on jets, including the paper by Hussain and Husain is for nozzles with no plug or centerbody within their exit planes. Several important engineering problems generate jets from nozzles which must include centerbodies. Separate-flow exhaust nozzles from jet engines would be but one example. The present work is an investigation into how the introduction of the centerbody changes the behavior of elliptic jets. The geometry of the nozzle was chosen to have a ratio of exit heights of three anticipating that past the centerbody tip the jet would coalesce into a 3:1 elliptical cross section. The actual cross section from this nozzle is quite different.

Experimental Facility and Procedure

The Gas Dynamics and Propulsion Laboratory at the University of Cincinnati (UC-GDPL) has a scale model of a separate-flow jet engine exhaust system. For the present experiment a new elliptic nozzle was designed and manufactured to mate with this existing and proven apparatus.

The design of the 3:1 elliptic nozzle (E30) is shown in Figure 3. It was designed so that the ratio of the exit heights h_1 to h_2 would be 3:1 with the expectation of producing a jet which would take on a 3:1 elliptic cross section downstream of the centerbody. The centerbody has a half-angle of 16° and extends $1.79D_{eq}$ beyond the exit plane of the nozzle.

The design was also intended to match the exit area, mass flow, and thrust of an existing round conical nozzle. The hardware is shown in Figure 4. Integrated velocity measurements have shown that the nozzle does indeed pass the same mass flow as a round nozzle of equal exit area at the same NPR and stagnation temperature.

Instrumentation

The principal tool in this investigation is a LaVision Stereoscopic PIV system. This instrument has been employed on the jet model previously and has proven effective at capturing three-component velocity measurements in any number of cross-stream planes. By taking an entire plane simultaneously we eliminate one source of measurement error; when using Constant Temperature Anemometry (CTA) or Pitot measurements the set-point of the jet will inevitably drift slightly while the probe is in motion. This superimposes this "tunnel drift" on top of the actual spatial variation in velocity field under study. By making a single shot simultaneous measurement, this drift is eliminated for an entire cross-cut.

The entire PIV suite, laser and both cameras are mounted on a traverse which allows the system to be translated, undisturbed, to any streamwise location allowing many cross-cuts to be measured without the loss of time in changing setups and without the uncertainties which come from repeated adjustment of components.

The PIV system takes multiple pairs of images, typically 200-500 pairs in a single run. From this we can get mean velocity in three components. We can also get turbulent statistics up to the frequency limit imposed by the integration time between images in a single pair. This can be rendered as *u'*, *v'*, *w'* or taken together in the form of Turbulent Kinetic Energy (TKE).

Results

In initial testing on this project we examined the conditions at the nozzle exit plane to assure ourselves that the flow is not separated in the nozzle and that the mass flow is the same as that of a round conical nozzle of equal area. Radii in the major and minor axis planes and also in planes 30° and 60° inclined from them were surveyed with a boundary layer pitot probe. The resulting total pressure contours were integrated and thrust was calculated. These measurements were compared with those from a round nozzle of equal exit area and the thrust and mass flow were found to be the same to within the measurement uncertainties.

The main focus of the present work was 3-D Stereo PIV in planes normal to the axis of the nozzle. Mean flow measurements are presented here. Examination of the turbulent data will be deferred to another paper. Examples of the velocities are shown in Figure 6. This figure shows the range of velocities examined. In both cases the measurement plane was $0.24D_{eq}$ downstream of the centerbody tip or $2.03D_{eq}$ downstream of the nozzle exit. Subfigure (a) shows a case where the control valve is only cracked, giving a maximum velocity of 96 m/s. Subfigure (b) shows the heated sonic case. This is the highest

velocity case measured, with a peak velocity of 360 m/s. As can be seen in subfigure (b) the laser illumination in the negative-x half of the jet was superior to the illumination in the positive-x plane. This lead to occasional disturbances in the positive-x half plane. For this reason the negative-x half plane was used in extracting profile data.

Across the whole range of velocities and temperatures the gross character of the jet remained the same. In every case the jet bifurcates. By the end of the centerbody tip the potential core has completely split and the two potential regions diverge as the jet spreads. There are subtle differences depending on temperature and nozzle pressure ratio, but the gross behavior was the same for all conditions tested.

Figure 7 shows the same two extreme cases represented as line plots of the mean velocity magnitude in the major axis plane. Also depicted by horizontal lines on each subfigure are the velocities, $u_{i,}$ predicted for isentropic quasi-1-D expansion. These velocities could be considered the perfect-nozzle velocities. It can be easily seen that these velocities closely match the velocities in the potential core region of each jet. Further data will be shown normalized by this perfect-nozzle velocity. It will be seen that this produces good data collapse in all cases.

We examine the effect of Nozzle Pressure Ratio (NPR) or Mach number in Figure 8 and Figure 9. In Figure 8 we see major axis velocity contours at an axial position of $0.24D_{eq}$ over a range of NPR from 1.4 to 1.89. The collapse of the data is strong. There are no discernable differences in the profiles at this location. In Figure 9 we examine the shape of the potential core region, which we take to be the region where $u/u_i > 90\%$. Here again the differences are very slight. We will look at how the size of this region evolves as we move downstream below, and we will begin to see slight variations between cycle conditions as the jet develops.

The development of the jet as it mixes past the centerbody tip is illustrated in Figure 10. As the flow moves downstream the mixing layer thickens, the velocity gradients become less steep and the potential cores shrink. It can be plainly seen that the centers of the potential cores also spread farther apart in x and that the potential regions remain wider than they are tall. (larger in x than in y).

We will look in detail at the shrinking of the $u/u_i = 90\%$ contour as an indicator of the length of the potential core, but we will also look at the decay of the maximum velocity. In an axisymmetric jet we would look first to the decay of the centerline velocity and expect that this velocity would remain steady throughout the potential region, and then the curve would exhibit a shoulder or kink as the mixing layers merge at the end of the potential core and the centerline velocity begins to decay. Since our potential cores do not follow the centerline, we must look at something else.

We expect by analogy that the center of each potential core would have a flat region of the velocity profile and that this flat region would be the maximum velocity. In Figure 11 we plot the maximum velocity as a function of axial position for two nozzle pressure ratios. We do see a generally flat region at the beginning and we do see a definite

downturn in this max velocity past z = $1.44D_{eq}$ or so. We do not see a clear shoulder or kink to clearly mark the end of the potential region. The velocities plotted here, like those presented above, are the magnitudes of the local velocities, not the streamwise velocity contours.

The major axis velocity contours for NPR = 1.80, T_0 = 220F are plotted in Figure 12. The contours range from axial positions from $0.48D_{eq}$ downstream of the centerbody tip to $3.36D_{eq}$. It is clear that the shear layers become less steep as they thicken. It can be seen that by z = $1.92D_{eq}$ there is no longer a region of the profile which is flat. This is an indication that the potential core region is gone. Finally it can be seen that the region of peak velocity moves away from the y axis as the jet develops.

The same conditions are shown in Figure 13. Here we again see that the potential core region moves away from the y axis as it develops. It also shrinks in both y and x. Beyond z = $2.40D_{eq}$ there is no region of velocity within 10% of the perfect-nozzle velocity. 90% of the perfect nozzle velocity is a generous allowance for the potential core region. A number closer to unity would be preferred. Higher values were tried as indicators of the potential core region, but noise in the data made them unworkable. It should be noted that the actual potential core is smaller than the 90% contours since the actual velocity cut-off is higher. The limits shown are thus outer bounds for the actual potential core.

Figure 14 and Figure 15 show the same plots for NPR = 1.50, T_0 = 220F. The trends are the same. The spreading of the shear layers, the reduction of the potential core regions, the shrinking of the potential core regions in the y direction are all evident. For the NPR = 1.50 case, the last contour of u/u_i = 90% shown in Figure 15 is for $1.92D_{eq}$ axial distance. While the difference is slight, this is suggestive of a shorter potential core for the lower NPR case.

The vertical and horizontal extents of the regions of velocity above 90% are shown in Figure 16 and Figure 17. Linear fits to the data are shown and the lines have been extended to show the trend in potential core length. Again it is worth noting, that since 90% velocity is less than the potential core velocity, the 90% contours will be larger than the actual potential core regions, and the potential core lengths will also be over-predicted. We may assume, though that these 90% contours will give a good indication of the trends and the trends we see here are that the potential core length shortens as the NPR goes down. We may also note that the lines for the vertical extent cross before those for the horizontal extent would. This tells us that the potential core will be extinguished when the shear layers in a constant x profile merge, not when the shear layers in a y = constant profile do.

Next we examine the velocity contours along constant x. The x locations for each contour were chosen to take the contour through the thickest part of the high velocity region as determined by the 90% velocity plots. Figure 18 shows the velocity profiles for NPR = 1.80, T_0 = 220F. From this plot we can see that the normalized velocity has a clear flat region for z = $0.48D_{eq}$ and $0.96D_{eq}$. The velocity peaks at a normalized velocity

of 1 for z = $1.44D_{eq}$. But by $1.92D_{eq}$ the velocity is not reaching the peak value. The potential core is thus ending before $1.92D_{eq}$ is reached. Figure 19 is much the same, again the potential core does not reach $1.92D_{eq}$.

In addition to investigating the effects of NPR or Mach number on the development of the jet from the elliptic plug nozzle we also looked at the effect of heating. Figure 20 shows 90% velocity contours for heated and unheated conditions. Subfigure (a) is for NPR = 1.80 and subfigure (b) is for NPR = 1.50. It can be plainly seen that in both cases the heated jet's 90% region is smaller in the y direction and is shifted farther from the x axis. Looking at Figure 21, however shows that the same trends exist when comparing NPR = 1.80 and NPR = 1.50 jets at the same temperature. In this case the higher speed jet has a 90% region which is thinner in y and shifted farther from the x axis. It is likely that what we are really seeing here are changes in velocity due to changes in the sound speed. It is impossible to confirm this hypothesis with the data in-hand however.

Discussion

The nozzle under study was originally designed with the naïve expectation that a nozzle with a 3:1 ratio of exit heights, would produce an elliptical potential region past the centerbody tip of approximately 3:1 aspect ratio. For aspect ratios below 4:1 Hussain and Husain found axis switching to be the dominant behavior of the jet. Bifurcation is the expected behavior of elliptic jets of aspect ratios above 4:1. So in one sense, it would appear that the introduction of a centerbody has increased the effective aspect ratio of our elliptic jet.

Looking at the mechanism of the process, however, it is clear that by the end of the centerbody tip, the shear layer from the elliptical nozzle outer edge, and boundary layer growing along the conical centerbody have merged in the minor axis plane extinguishing the potential core in this area. While there may be some 3-D evolution of the vortex rings going on as discussed in Hussain & Husain, the dominant cause of bifurcation in this case is likely to be the merger of these two shear layers.

The greatest difference between round plain nozzles and round plug nozzles is, obviously enough, the presence of the centerbody or plug in the latter case. Another less obvious difference has to do with a radial component of velocity. The centerbody in most such nozzles is conical, as ours is. In order to have the flow exit tangent to this conical surface, the inner surface of the nozzle is also conical, having a negative slope in the r-z plane and imparting a component of velocity in the negative r direction. In building our elliptical nozzle we varied the exit heights, and also the degree of negative slope at the exit to the nozzle. Examining Figure 3 (b) and (c) one can plainly see that this negative slope at the exit is grossly different in the major and minor axis planes. In the major axis plane the slope is nearly zero, while in the minor axis plane the slope is steeper than it would be for a corresponding round nozzle.

It has been suggested that the mechanism may not only be growth and merger of the inner boundary layer and outer shear layer, but also the driving of the shear layer into the plug by this inward component of velocity (Richard Cedar, private communication).

In order to determine with certainty what is driving the rapid merger between the nozzle lip shear layer and the centerbody boundary layer we need additional measurements upstream of the centerbody tip. Some initial PIV measurements were made in this region, but the resolution was too low to be usable. We intend to repeat these measurements with greater magnification on the cameras, and expect this data to shed light on the behavior in this region.

Further Work

The present paper examines the mean flow data for this class of flows. In fact it is concerned exclusively with the velocity magnitude values without considering the individual orthogonal components of velocity. These remain to be examined as do the distributions of vorticity, Turbulent Kinetic Energy (TKE) and other turbulent statistics. In addition to examining the data already in-hand and taking additionally PIV upstream of the centerbody tip, we intend to measure the shear and wake regions with hot wire or Laser Doppler Anemometry (LDA). Since jet behavior has been shown to be sensitive to the boundary layer thickness distributions at the exit, this data is likely to be significant.

References

Crow, S. C. & Champagne, F. H. 1971. Orderly structure in jet turbulence. *J. Fluid Mech.* 48:547-591.

Ho, C-M. & Gutmark, E. 1987. Vortex induction and mass entrainment in a small-aspect-ratio elliptic jet. *J. Fluid Mech.* 179:383-405.

Hussain & Husain. 1989. Elliptic Jets. Part 1: Characteristics of unexcited and excited jets. *J. Fluid Mech.* 208:257-320.

Krothapalli, A., Baganoff, D. & Karamcheti, K. 1981. On the mixing of a rectangular jet. *J. Fluid Mech.* 107:201-220.

Wygnanski, I. & Fiedler, H. E. 1969. Some measurements in the self-preserving jet. *J. Fluid Mech.* 38:577-612.

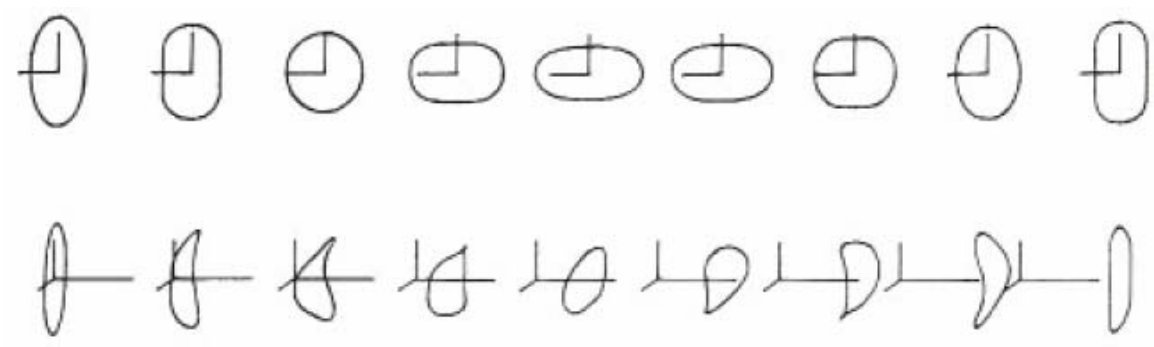

Figure 1 Axis switching mechanism (Figure from Hussain & Husain 1989).

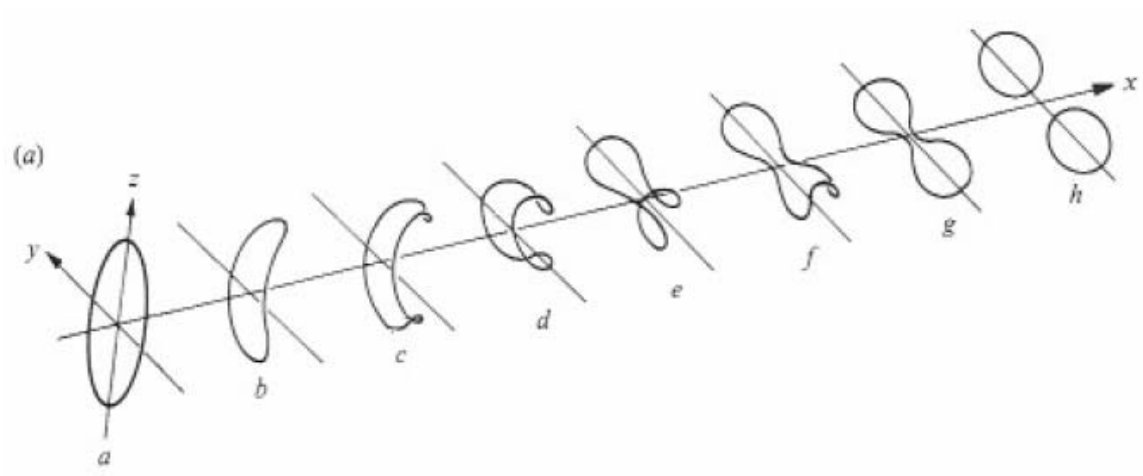

Figure 2 Jet Bifurcation mechanism (Figure from Hussain & Husain 1989).

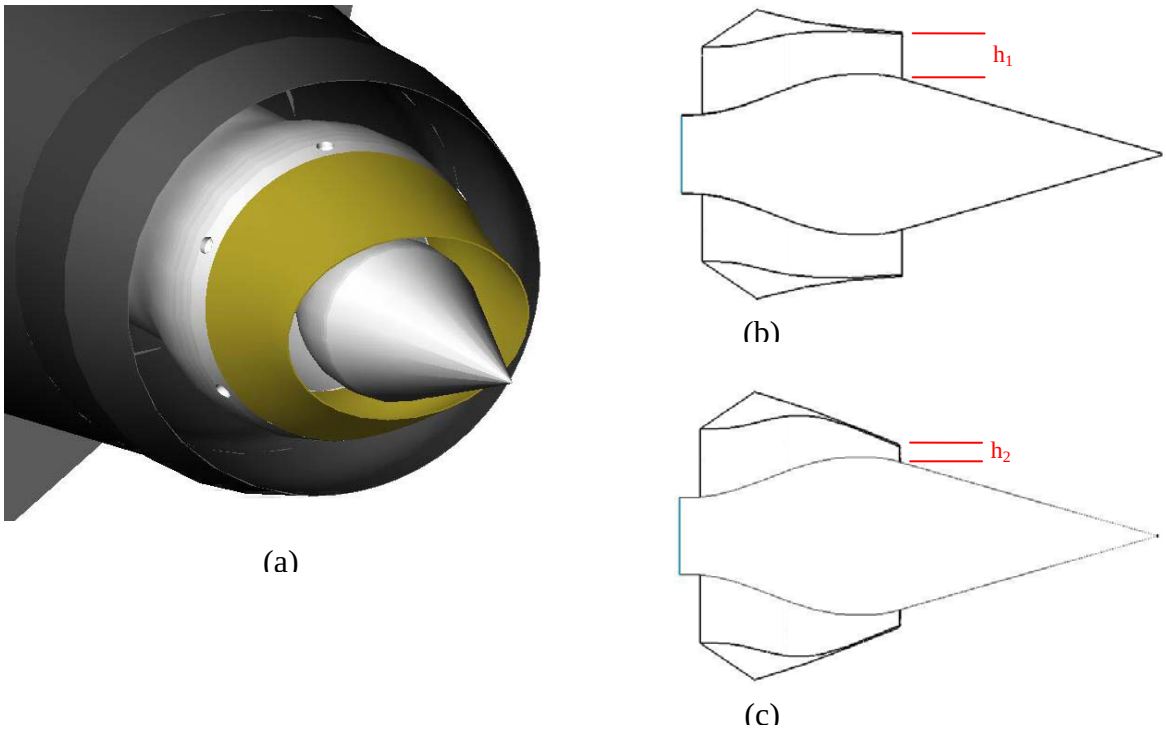

Figure 3 – 3:1 Elliptical nozzle with centerbody. (a) Perspective view of complete assembly. (b) Major axis cross section. (c) Minor axis cross section. An elliptic nozzle was fabricated to fit UC-GDPL's existing coaxial jet model. The 3:1 ratio is the ratio of the outlet heights $h_1 = 3h_2$.

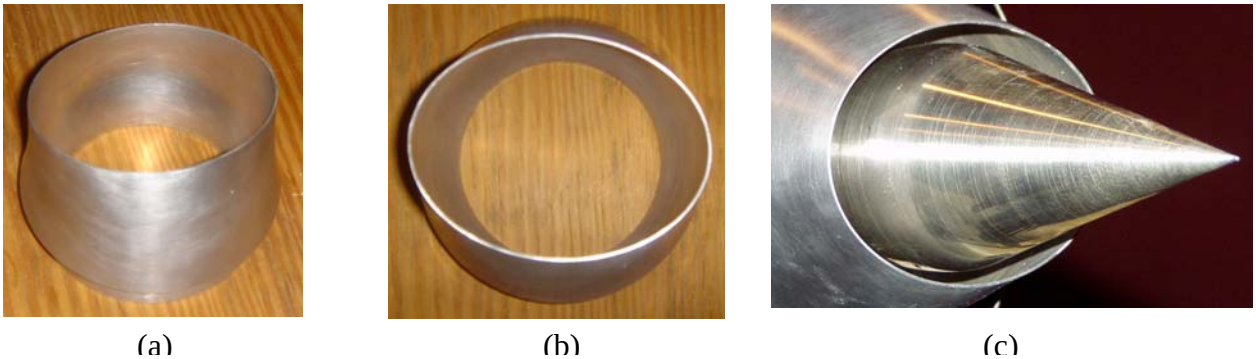

Figure 4 – 3:1 Elliptical nozzle hardware.. (a) New nozzle, perspective view, (b) New nozzle end view, (c) New nozzle assembled.

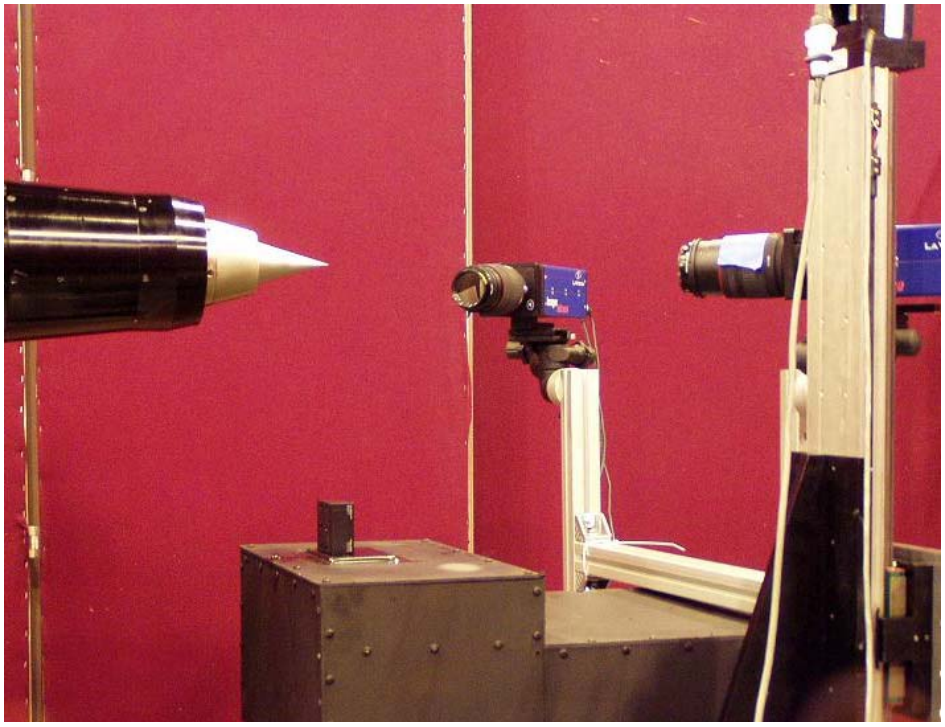

Figure 5 – Stereo Particle Image Velocimetry setup. This system allows simultanous capture of three-component velocity in a cross-stream plane. Simultaneous capture eliminates unceetainties introduced by set-point drift in NPR or temperature. The laser and both cameras are mounted on a large 3-D manual traverse. This allows the entire setup to be translated, undistrurbed, to several streamwise locations.

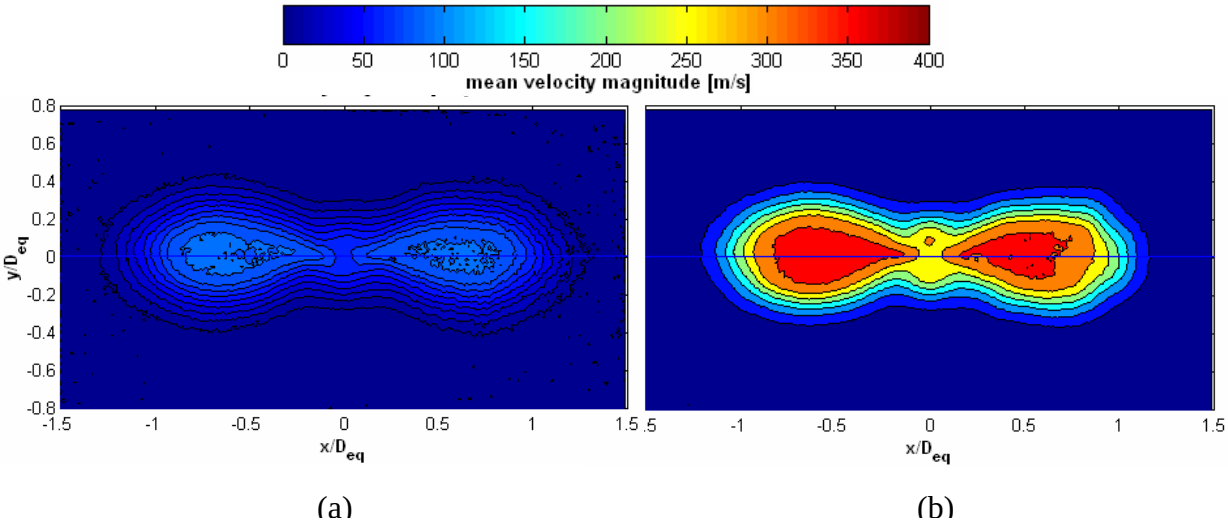

Figure 6 – Velocity magnitude contours measured in a plane $0.24D_{eq}$ downstream of the centerbody exit. The horizontal line through each plot is the major axis plane, along which velocity line plots will be extracted. (a) Lowest velocity case, 100 m/s. (b) Highest velocity case, sonic flow at T_0 = 220F, 358 m/s.

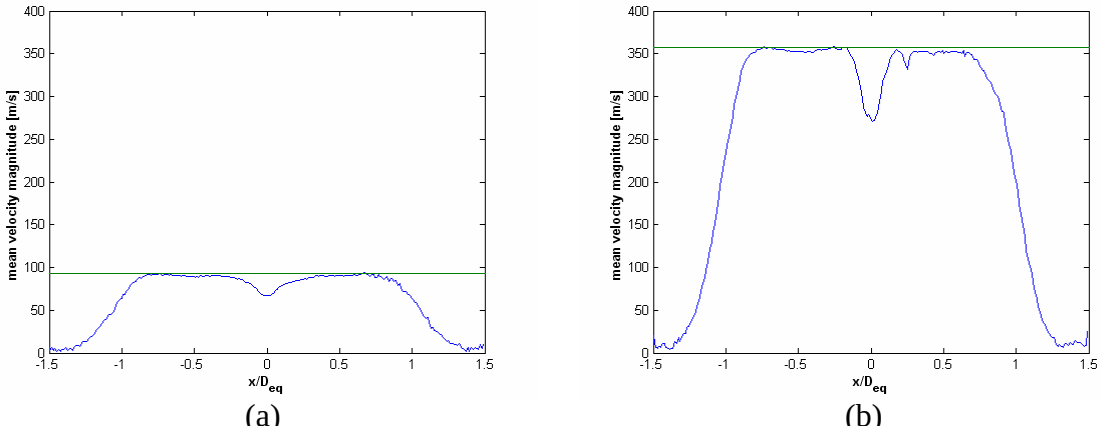

Figure 7 – Velocity along the major axis at an axial position $0.24D_{eq}$ downstream of the centerbody tip. The horizontal lines are the velocities for a perfect nozzle at the same NPR and T_0. This is a reasonable approximation to the potential core velocity. In subsequent plots, velocities will be normalized by this value. (a) Lowest velocity case, 100 m/s. (b) Highest velocity case, sonic flow at T_0 = 220F, 358 m/s.

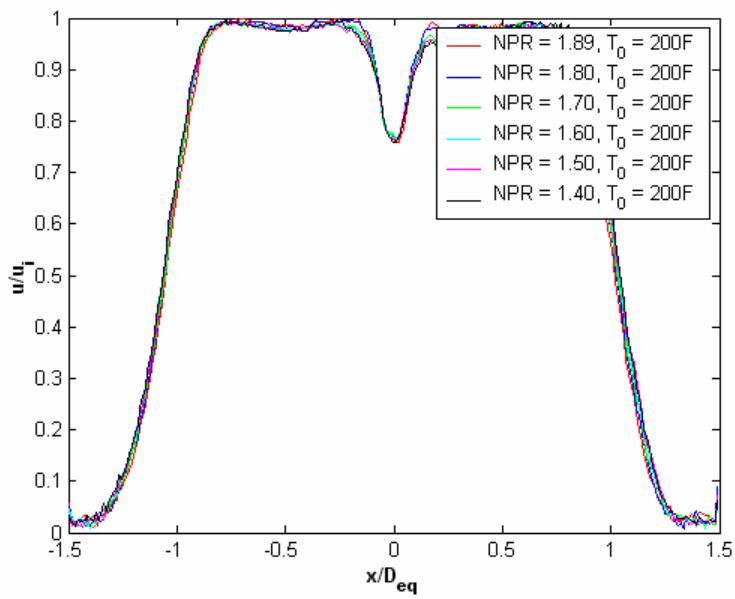

Figure 8 – Normalized mean velocity magnitude plots along the major axis at an axial location $0.24D_{eq}$ downstream of the centerbody tip. The velocity profiles are relatively insensitive to NPR or Mach number.

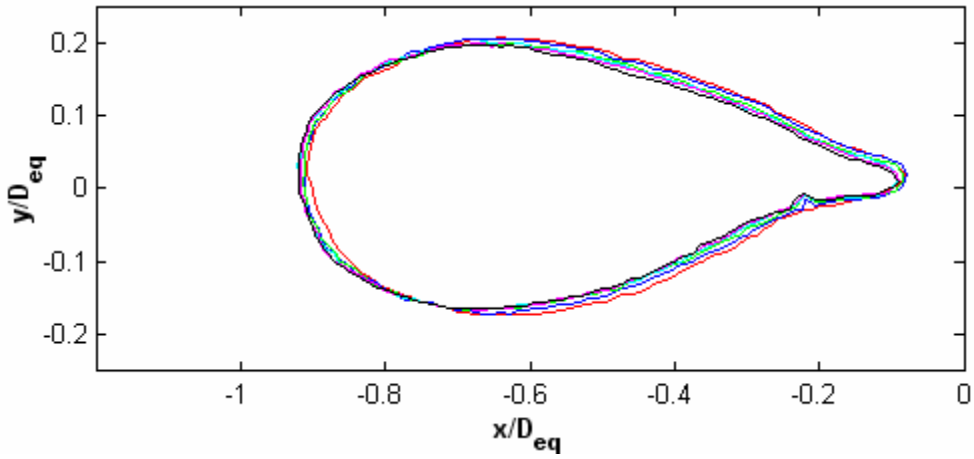

Figure 9 – Contours of u/u_i = 90%. This value is taken as a proxy for the edge of the potential core region. Legend same as previous figure. Again we see little sensitivity to NPR or Mach number.

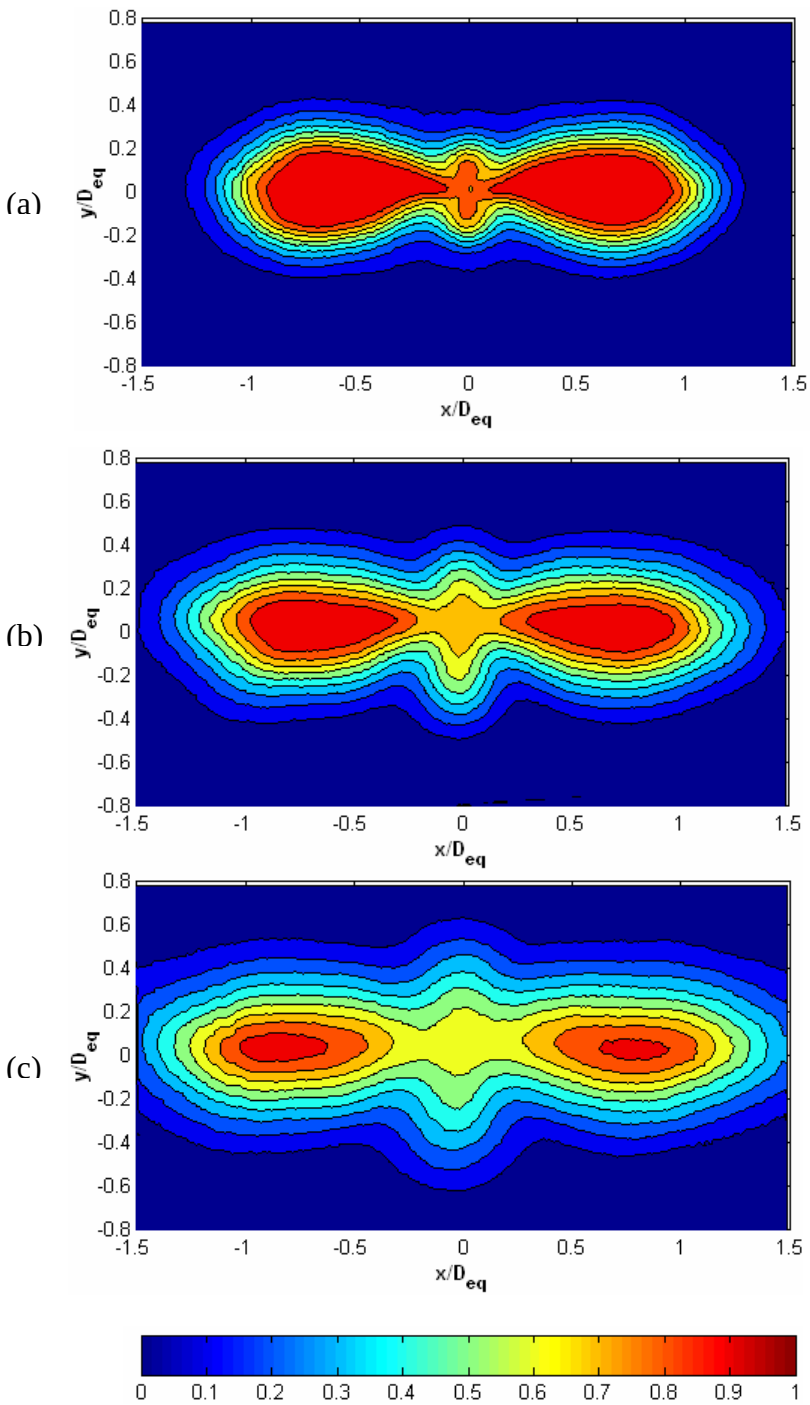

Figure 10 – Streamwise development of the flow-field as shown by normalized mean velocity magnitude contours in planes normal to the nozzle centerline. For all cases NPR = 1.80, T_0 = 220F. The highest contour in each case is u/u_i = 90%. This contour will be taken as indicative of the potential core region in subsequent plots. (a) axial position 0.48D_{eq} downstream of centerbody tip. (b) 1.44D_{eq} downstream of tip. (c) 2.40D_{eq} downstream of tip.

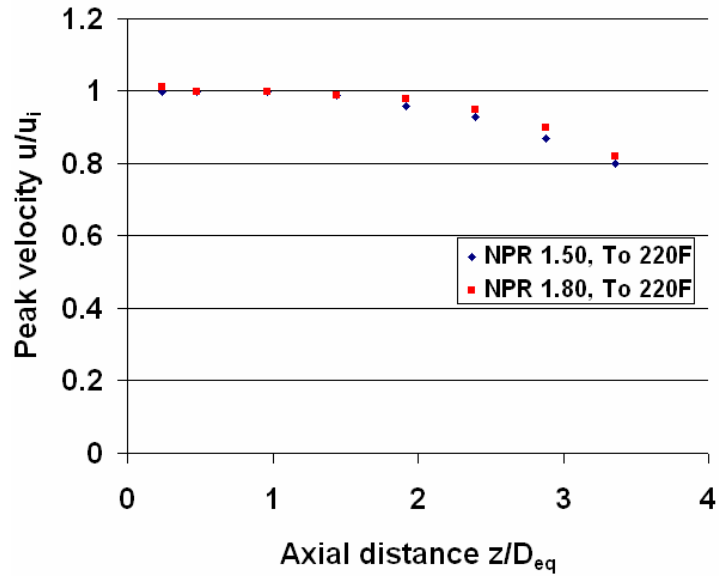

Figure 11 – Peak velocities as a function of axial position. Since centerline velocity is not in the potential core region we look at the decay of the peak velocity as an indication of the end of the potential core. While we do not see a clear sholder in the curve we can tell that for both Nozzle Pressure Ratios the potential core seems to have decayed past 2 equivalent diameters or so.

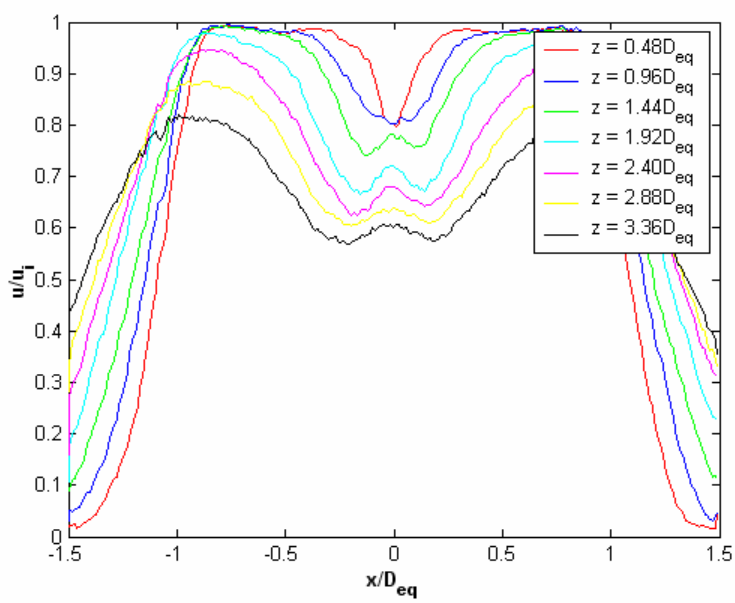

Figure 12 – Normalized mean velocity magnitude plots for NPR = 1.80, To = 220F along the major axis at axial locations ranging from $0.48D_{eq}$ to $3.36D_{eq}$.

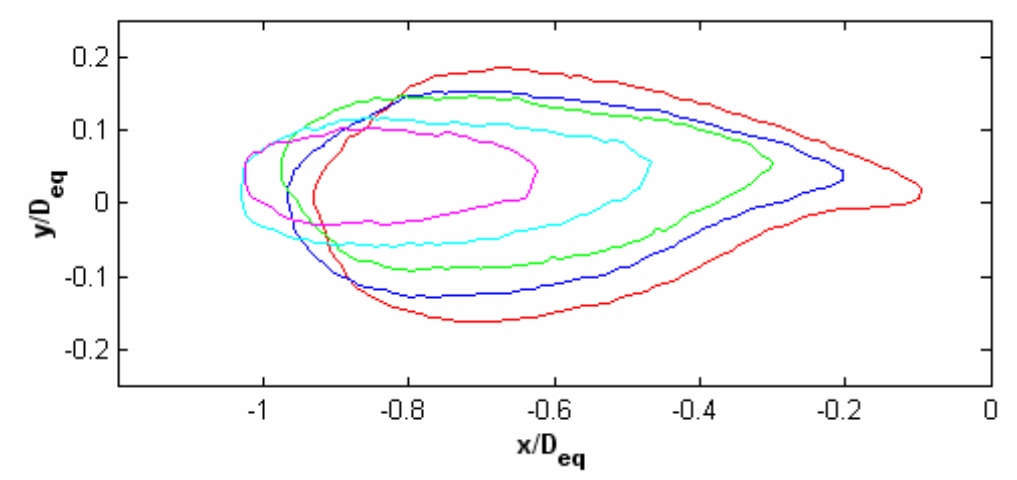

Figure 13 – Contours of u/u_i = 90% for NPR = 1.80, To = 220F at axial locations ranging from $0.48D_{eq}$ to $3.36D_{eq}$. For legend, see previous figure.

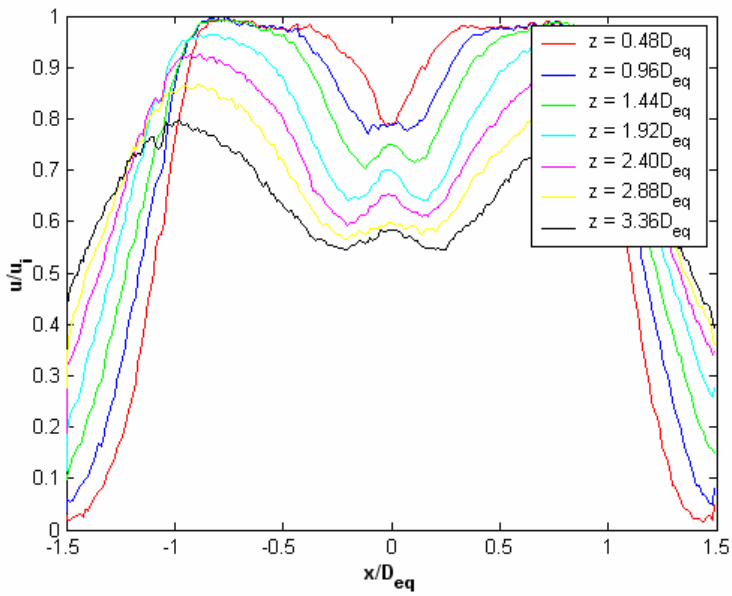

Figure 14 – Normalized mean velocity magnitude plots for NPR = 1.50, To = 220F along the major axis at axial locations ranging from $0.48D_{eq}$ to $3.36D_{eq}$.

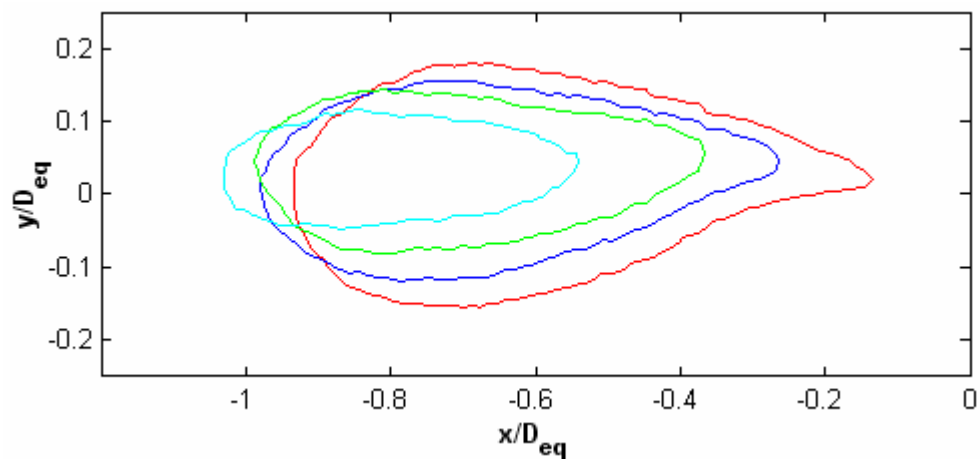

Figure 15 – Contours of u/u_i = 90% for for NPR = 1.50, To = 220F at axial locations ranging $0.48D_{eq}$ to $3.36D_{eq}$. For legend, see previous figure.

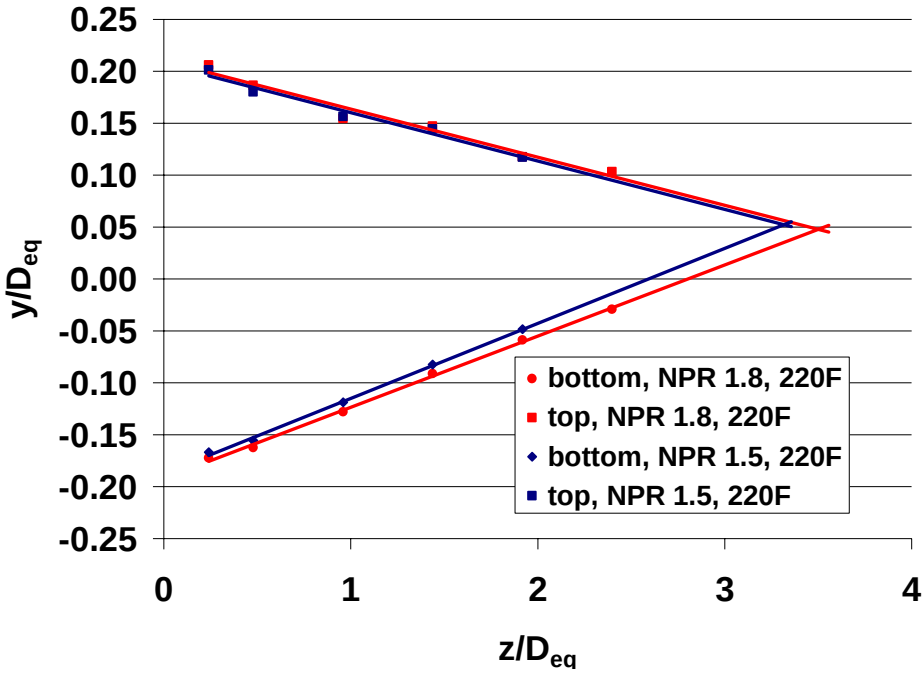

Figure 16 – Vertical edges of the 90% velocity region.

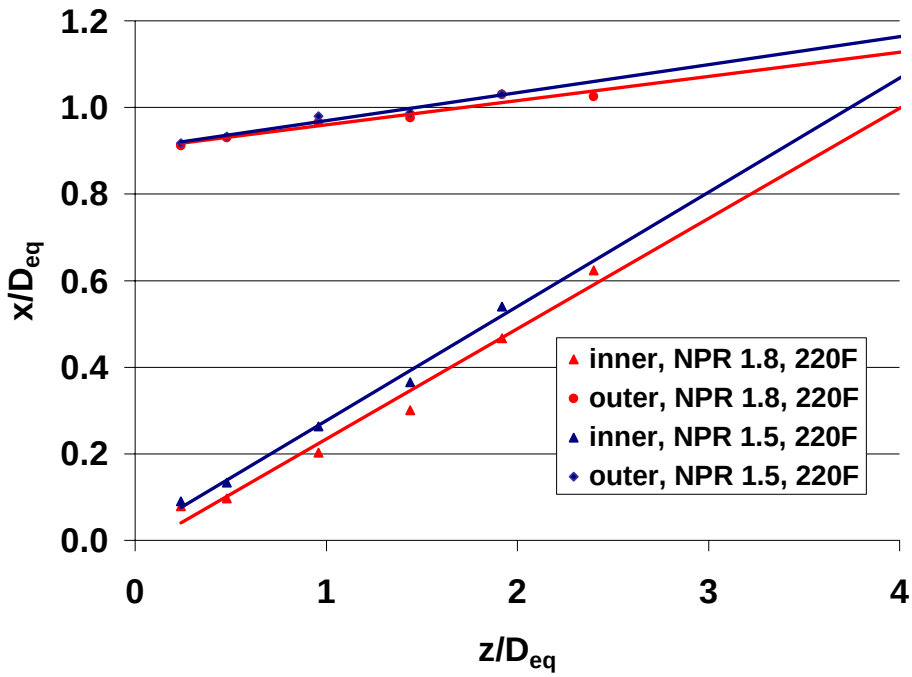

Figure 17 – Horizontal edges of the 90% velocity region.

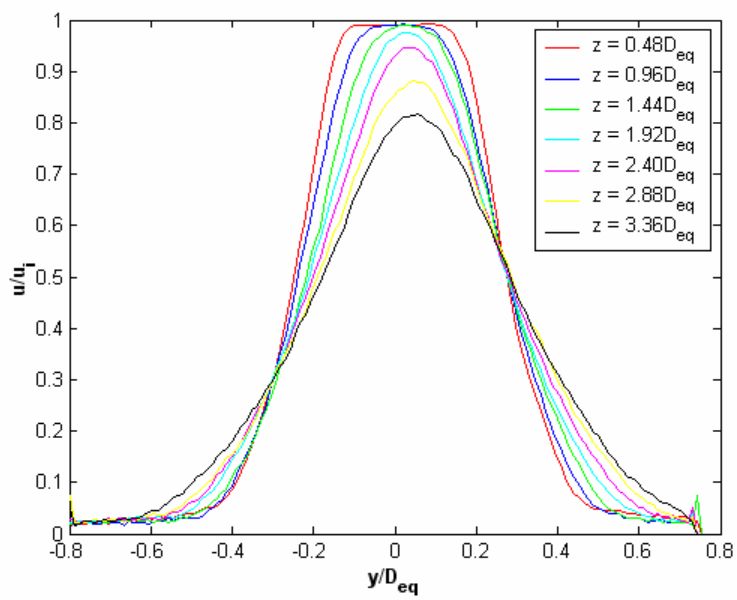

Figure 18 – Velocity profiles for NPR = 1.80, To = 200F along lines of constant x and constant z. The y values were chosen to pass through the thickest part of the 90% velocity contours.

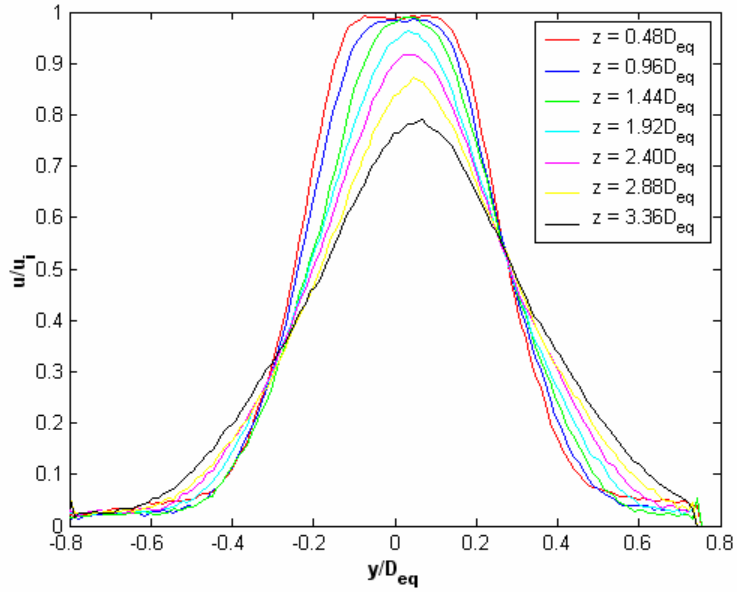

Figure 19 – Velocity profiles for NPR = 1.50, To = 220F along lines of constant x and constant z. The y values were chosen to pass through the thickest part of the 90% velocity contours.

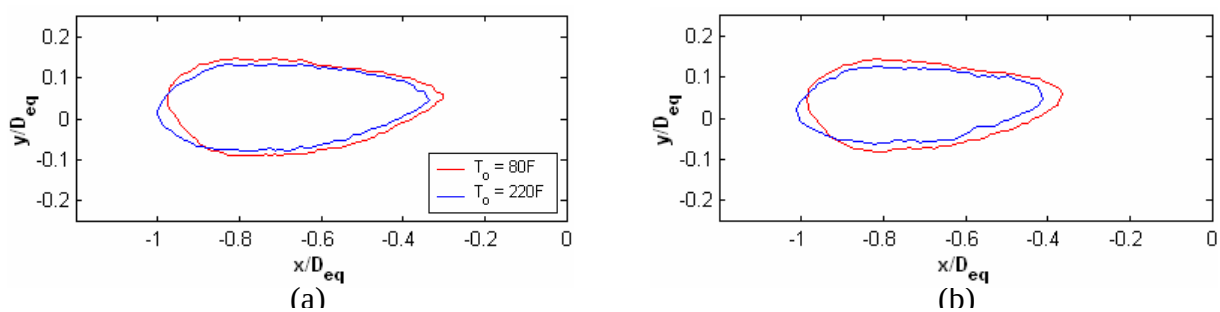

Figure 20 – 90% velocity contours at an axial position z = 1.44D_{eq} downstream of centerbody tip. (a) NPR = 1.80. (b) NPR = 1.50

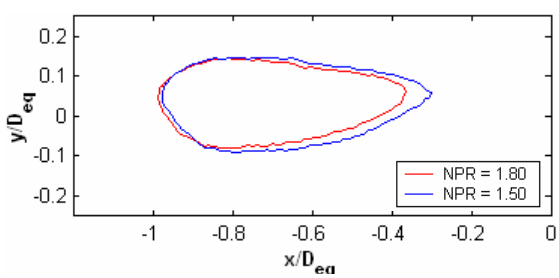

Figure 21 – 90% velocity contours at an axial position z = 1.44D_{eq} downstream of centerbody tip To = 220F.